ISSN 1392-1320 MATERIALS SCIENCE (MEDŽIAGOTYRA). Vol. XX, No. X. 2027

Experimental Study on Chemical Polishing and Etching Solutions for Metallographic Testing of P91 Steel

Lin WANG [1], Yuchang Li [1], Bo ZHAO [2], Sibei LIU [3], Yue GAO [4], Chunlei ZHONG [2], Yaxia LI [1] *

[1] *Shenyang University of Chemical Technology, School of Mechanical and Power Engineering, 110142, Shenyang*
[2] *Dalian Boiler and Pressure Vessel Inspection and Research Institute Co., Ltd., Energy Conservation and Emission Reduction Room, 116083, Dalian*
[3] *Hunan Special Equipment Inspection and Testing Research Institute, Comprehensive Management Office, 410116, Changsha*
[4] *Liaoning Ecological Environment Monitoring Center, Monitoring and Analysis Room, 110015, Shenyang*

http://doi.org/10.5755/j02.ms.45056

Received 19 May 2026; accepted 1 July 2026

To meet the demand for rapid and high-quality metallographic specimen preparation of P91 steel, this study systematically optimized the chemical polishing and etching processes through full-factorial and single-factor experiments. The results indicate that the optimal formulation for the chemical polishing solution is 20 ml of hydrogen peroxide, 1.75 g of ammonium hydrogen fluoride, 2.0 g of oxalic acid, and 25 ml of deionized water. The optimal process parameters involve pre-grinding up to 600-grit, followed by chemical polishing at 25 °C for 120 s. Scanning Electron Microscopy (SEM) and Energy Dispersive X-Ray Spectroscopy (EDX) analyses demonstrate that this optimized process effectively disrupts temporary chromium-rich passivation films and promotes a dynamic oxidation-dissolution equilibrium. This mechanism helps to prevent localized over-corrosion and effectively retains critical secondary-phase precipitates, such as Cr-Mo-rich carbides. Furthermore, combining this polishing process with an optimized ethanol-buffered etchant (20 ml HCl + 100 ml anhydrous ethanol) clearly reveals the lamellar tempered martensite microstructure of P91 steel while mitigating severe matrix degradation. By avoiding the deformation layers typically introduced by mechanical polishing, this high-fidelity approach provides an efficient and reliable sample preparation methodology for on-site microstructural examination, thereby supporting the subsequent evaluation of critical pressure-bearing components.
Keywords: P91 steel, chemical polishing, etching solution, metallographic inspection, microstructure.

1. INTRODUCTION

P91 steel (10Cr9MoVNb) [1], microalloyed with V, Nb, and N [2], possesses exceptional high-temperature creep strength and microstructural stability [3], making it a vital structural material for critical pressure-bearing components in power and petrochemical industries [4 – 6]. Under typical operating conditions (570 – 625 °C, 25 – 30 MPa), its microstructural state directly governs long-term operational safety [7]. Therefore, precisely characterizing its microstructural evolution is an essential prerequisite for reliable service life assessment.

Metallographic examination [8] remains the primary method to analyze P91 steel, where polishing and etching are fundamental steps. Current preparation techniques include mechanical [9], laser [10], chemical [11], and electrochemical polishing [12, 13]. However, mechanical polishing creates deformation layers, while advanced alternatives are constrained by high costs, equipment complexity, or toxicity. Furthermore, conventional etchants often cause blurred martensitic boundaries, hindering accurate evaluation. Given the strict spatial and environmental constraints of on-site inspections, developing an optimized, equipment-independent chemical polishing and etching system is a critical technological direction.

Chemical polishing relies on selective surface dissolution to eliminate machining marks and oxide layers across various engineering alloys, including zirconium [14] and stainless steels [15]. However, its systematic optimization for the rapid in-situ preparation of P91 steel remains insufficiently explored, especially regarding solution formulation and etchant compatibility. Consequently, this study utilizes full-factorial and single-factor experiments to systematically investigate the polishing formulations, process parameters, and etching compatibility. By optimizing a stress-free chemical polishing and etching system for P91 steel, this work overcomes the deformation issues of mechanical polishing and the equipment constraints of electrochemical methods. Ultimately, this study provides a high-fidelity approach for microstructural characterization, offering a reliable and efficient methodology for the on-site service life assessment of critical thermal power plant components.

2. EXPERIMENTAL DETAILS

2.1. Materials and process flow

The study focused on P91 steel tubes with a diameter of 60.3 mm and a length of 1 m. The chemical composition is shown in Table 1, and the process flow is as follows: Coarse

* Corresponding author: Y. Li
E-mail: *liyaxia@syuct.edu.cn*

grinding→Fine grinding→Chemical polishing→Etching→ Observation. The process flow diagram is shown in Fig. 1.

Table 1. Chemical composition of P91 steel (wt.%)

C	Si	Mn	Cr	Mo	V	Nb	N
0.11	0.27	0.40	8.55	0.91	0.2	0.077	0.051

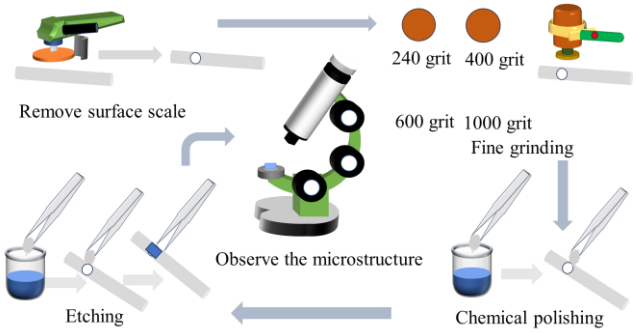

Fig. 1. Metallographic inspection process (chemical polishing)

In this process, coarse grinding involves using an angle grinder to remove the outermost oxide layer from the steel tube, while fine grinding involves sequentially grinding the surface using sandpaper of different grits (120-grit, 320-grit, 600-grit, 1000-grit) with a hand-held grinder. The basic process conditions are as follows: polishing temperature 20 – 35 °C, polishing time 30 – 150 s, and fine grinding up to 1000-grit.

2.2. Theoretical mechanism of the chemical polishing system

The selected H_2O_2-NH_4HF_2-$H_2C_2O_4$ system constitutes a synergistic chemical polishing process primarily involving oxidation, complexation, and dissolution. Using deionized water as a stable mass transfer medium, the core mechanism on the P91 steel surface involves three interconnected stages:

2.2.1. Oxidation and surface activation

Hydrogen peroxide (H_2O_2) acts as the primary oxidant, converting the P91 steel surface from a metallic to an ionic state, providing the fundamental driving force for material removal:

$$Fe + H_2O_2 + 2H^+ \rightarrow Fe^{2+} + 2H_2O; \quad (1)$$

$$2Fe^{2+} + H_2O_2 + 2H^+ \rightarrow 2Fe^{3+} + 2H_2O. \quad (2)$$

2.2.2. Film breakdown and primary complexation

Ammonium hydrogen fluoride (NH_4HF_2) acts as the activator. The F^- ions breach the dense, chromium-rich passivation film typical of P91 steel and form stable complexes with Fe^{3+} and Cr^{3+} ions, inducing a dynamic cycle of "film formation – dissolution – fresh substrate exposure":

$$Fe^{3+} + 6F^- \rightarrow [FeF_6]^{3-}; \quad (3)$$

$$Cr^{3+} + 6F^- \rightarrow [CrF_6]^{3-}; \quad (4)$$

$$Cr_2O_3 + 12F^- + 6H^+ \rightarrow 2[CrF_6]^{3-} + 3H_2O. \quad (5)$$

2.2.3. Secondary complexation and reaction regulation

Oxalic acid ($H_2C_2O_4$) is introduced as a buffer and secondary complexing agent to prevent excessively rapid localized reactions. By forming soluble oxalates, it facilitates product migration and prevents secondary deposition:

$$Fe^{3+} + 3H_2C_2O_4 \rightarrow [Fe(C_2O_4)_3]^{3-} + 6H^+; \quad (6)$$

$$Cr^{3+} + 3H_2C_2O_4 \rightarrow [Cr(C_2O_4)_3]^{3-} + 6H^+. \quad (7)$$

2.3. Performance testing

A TR200 surface roughness tester from Beijing Jitai Keji Testing Equipment Co., Ltd. was used to measure the surface roughness (*Ra*) of the P91 steel surface before and after chemical polishing, with the measured values recorded and statistically analyzed.

An AE2000MET inverted metallurgical microscope from McAudy Industrial Group Co., Ltd. was used to observe the surface morphology and metallographic structure of the finely ground P91 steel.

A ZEISS GeminiSEM 300 scanning electron microscope (Carl Zeiss, Germany) equipped with an Energy Dispersive X-Ray Spectroscopy (EDX) detector was employed for high-resolution observation of the surface morphology and micro-compositional analysis (including elemental mapping and point analysis) of the polished and etched specimens.

3. RESULTS AND DISCUSSION

3.1. Full-factorial experimental optimization of the chemical polishing solution formulation

At a temperature of approximately 25 °C and a polishing time of 90 s, using 25 ml of deionized water, the composition of the polishing solution was optimized using a 3^3 full factorial design, with the volume of hydrogen peroxide and the mass of ammonium hydrogen fluoride and oxalic acid in the solution as factors. The reduction in surface roughness of the samples following chemical polishing was used as the performance indicator. The level settings are shown in Table 2, and the results of the full factorial experiment are presented in Fig. 2 a.

Table 2. Factors and levels in the full-factorial design

Level	Factor		
	A:H_2O_2, ml	B:NH_4HF_2, g	C:$H_2C_2O_4$, g
1	20	1.50	1.5
2	30	1.75	2.0
3	40	2.00	2.5

Based on data from 27 sets of full-factorial experiments, the highest reduction in surface roughness (35.4 %) was achieved when the polishing solution consisted of 20 ml H_2O_2, 1.75 g NH_4HF_2 and 2.0 g $H_2C_2O_4$ (Group No.5); the surface scratches on the test specimens became noticeably shallower and smoother, yielding the best polishing results.

Formulations yielding poor polishing results (such as those with excessively high H_2O_2 and low acidity, or high acidity and low H_2O_2) result in a roughness reduction rate of only 11 % – 13 %.

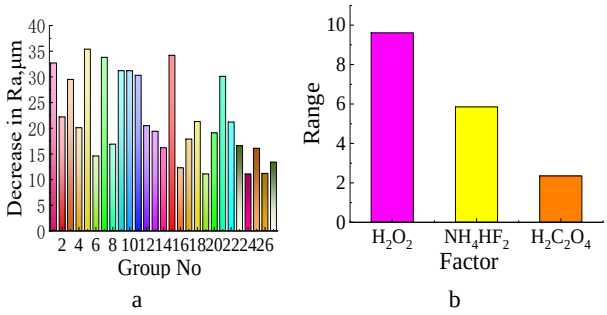

Fig. 2. Analysis of experimental effect for full factorial design: a – reduction in roughness from a full factorial experiment; b – range of each factor

The primary reasons for this are as follows: when there is an excess of oxidizing agent and insufficient acidity, surface oxides cannot be dissolved in a timely manner, leading to the formation of a residual film; conversely, when there is insufficient oxidizing agent and excessive acidity, over-etching occurs, resulting in uneven metal dissolution. It is evident, therefore, that there is a significant synergistic effect among H_2O_2, NH_4HF_2, and $H_2C_2O_4$ (which provide H^+ and complexation) [16]. The optimal surface finish achieved in Group No. 5 can be attributed to a favorable balance within the oxidation-dissolution synergy. At this specific ratio, the rate of metal oxidation induced by H_2O_2 appears to align well with the dissolution and complexation rates facilitated by F^- (as modeled in Eq. 1 and Eq. 3). Such a proportion promotes a steady-state dynamic equilibrium between the formation and subsequent dissolution of the surface oxide layer, ensuring that the localized mass transfer of reactants and products remains stable across the complex multiphase microstructure, thereby preventing both passivation-induced residual films and acid-driven over-etching to yield the optimal chemical polishing effect. A range analysis of the experimental results is shown in Fig. 2 b. Factor A (hydrogen peroxide) exhibited the largest range, at 9.61, followed by Factor B (ammonium hydrogen fluoride) with a range of 5.85, while Factor C (oxalic acid) had the smallest range, at 2.35. Consequently, the order of influence of each factor on the rate of roughness reduction is: A (hydrogen peroxide) >B (ammonium hydrogen fluoride) >C (oxalic acid).

3.2. The effect of polishing solution temperature on polishing quality

Temperature is a key parameter influencing the reaction rate of chemical polishing. Under fixed formulation conditions (20 ml hydrogen peroxide, 1.75 g ammonium hydrogen fluoride, 2.0 g oxalic acid, 25 ml deionized water) and a polishing time of 90 s, the effect of temperature within the range of 10 to 40 °C on the surface roughness of P91 steel was investigated. The experimental results are shown in Fig. 3. As the temperature rises, the reduction in surface roughness Ra exhibits a trend of initially increasing and then decreasing.

Within the 15 – 25 °C range, the reduction in *Ra* gradually increases. This can be explained by the thermal activation of the system: moderate temperature elevation effectively lowers the activation energy barrier, promoting the preferential dissolution of micro-protrusions and enhancing the overall leveling effect [17]. However, at temperatures exceeding 25 °C, the surface quality deteriorates. This behavior is primarily due to the accelerated decomposition of H_2O_2 and an uncontrollably rapid reaction rate. Such conditions disrupt the delicate passive-dissolution dynamic, shifting the uniform polishing process toward aggressive localized over-corrosion driven by uncontrolled redox kinetics and rapid gas evolution at the liquid-solid interface [18] and ultimately reducing microscopic flatness.

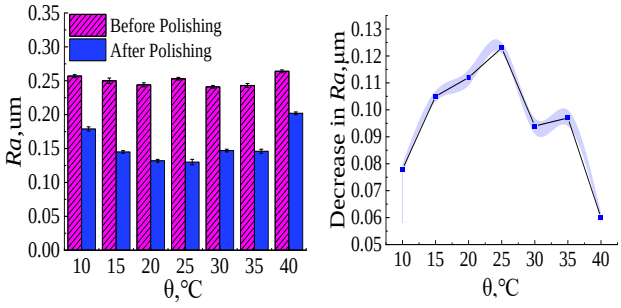

Fig. 3. Effect of different temperature on *Ra*: a – surface roughness before and after polishing; b – reduction in surface roughness after polishing

3.3. Effect of polishing time on polishing quality

The polishing time determines the amount of metal dissolved from the surface. If the time is too short, surface scratches cannot be completely removed; if the time is too long, it may lead to over-etching or the formation of pitting. Under a fixed formulation and at a temperature of 25 °C, the effect of polishing time (30 – 150 s) on surface quality was investigated, and the results are shown in Fig. 4. At 30 s, the removal rate was low; this may be attributed to the fact that, during the initial stage of polishing, the surface oxide film and impurities had not yet been fully removed, the reaction was in its induction phase, and the synergistic effect of oxidation and dissolution had not yet been fully established.

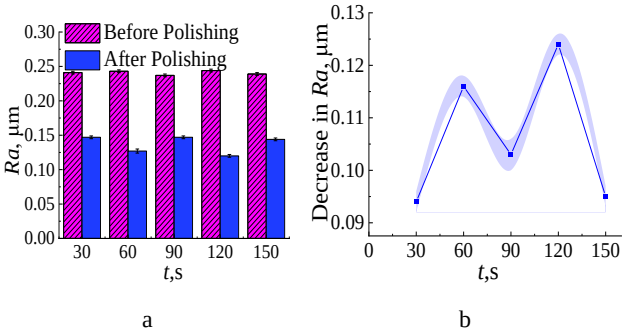

Fig. 4. Effect of different time on *Ra*: a – surface roughness before and after polishing; b – reduction in surface roughness after polishing

As the duration increased to 60 s, the removal rate rose significantly; at this point, the surface barrier layer was broken down, allowing the polishing solution to come into full contact with the substrate, and the synergistic effect of oxidation and complexation-dissolution entered a highly efficient state, markedly accelerating the removal rate.

Between 60 and 90 s, the removal rate declined slightly. To investigate the potential chromium enrichment within passive regions, EDX mapping and point analysis were performed to track the micro-compositional evolution. As illustrated in the upper panels of Fig. 5 a and b, the elemental maps clearly revealed localized, high-concentration clusters of Oxygen (O) and Chromium (Cr). EDX point analysis further quantified this localized Cr concentration at an anomalous 17.76 % (significantly exceeding the nominal 8.55 %). This direct evidence confirms that during this intermediate stage, the inherent tendency of high-chromium alloys leads to the formation of a dense, Cr-rich temporary passivation film, which restricts continuous material removal [19].

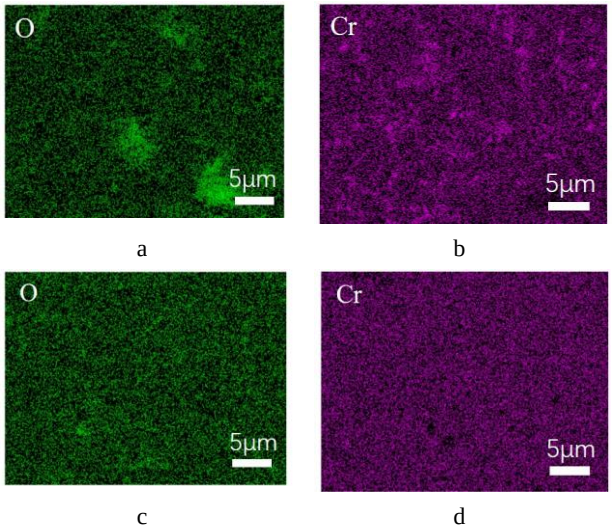

Fig. 5. Comparative EDX elemental mapping of the P91 steel surface at different polishing times: a – O distribution at 90 s; b – Cr distribution at 90 s; c – O distribution at 120 s; d – Cr distribution at 120 s

However, between 90 and 120 s, the sustained oxidation and complexation effectively disrupt this temporary barrier. As demonstrated in the lower panels of Fig. 5 c and d, the optimally polished surface transitions to a highly uniform distribution of O and Cr, with the Cr concentration returning to a baseline of 8.76 % (confirmed by point analysis). This striking contrast provides robust empirical evidence that the optimized F^- concentration successfully breaches the passive layer and establishes a steady-state dynamic equilibrium, effectively eradicating detrimental chromium enrichment and exposing the fresh substrate for optimal leveling.

However, between 120 and 150 s, the removal rate declines again. This late-stage deterioration is governed by classic dissolution kinetics and localized corrosion mechanisms [20]. As the treatment is prolonged, the localized activity of the solution decreases due to H_2O_2 decomposition and the depletion of active ions (F^- and $C_2O_4^{2-}$), weakening the complexation reactions (Eq. 4 and Eq. 7). This imbalance disrupts the steady-state dissolution, causing the uniform polishing process to transition into aggressive localized attacks. As shown in Fig. 6, while the carbide precipitates (bright particles) remain dispersed, the matrix suffers from uncoordinated localized corrosion, resulting in distinct, randomly distributed micro-pits (dark voids). This severe localized pitting disrupts the structural integrity of the surface and accounts for the significant drop in the effective uniform removal rate.

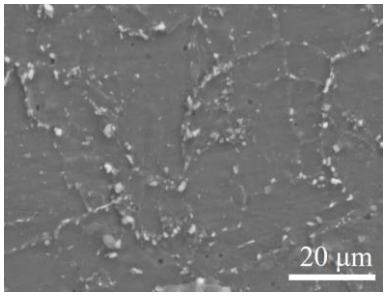

Fig. 6. SEM morphology of the over-polished P91 steel surface (150 s)

3.4. The effect of sandpaper grit size on polishing quality

Chemical polishing can effectively improve the micro-surface flatness of specimens, but its ability to remove macro-scratches is limited; therefore, the precision of the pre-treatment process will directly affect the final polishing result. To investigate the effect of sandpaper grit size on the quality of chemical polishing, under fixed process conditions, namely a polishing temperature of 25 °C and a polishing time of 120 s, P91 steel specimens were subjected to stepwise fine grinding pretreatment using 120-grit, 320-grit, 600-grit and 1000-grit sandpaper. This was followed by chemical polishing, after which the surface roughness *Ra* of the specimens was measured, while the surface morphology following polishing was examined using a Scanning Electron Microscope (SEM).

The experimental results are shown in Table 3. As can be seen from the table, as the grit size of the pre-treatment sandpaper increased, the initial roughness prior to chemical polishing decreased significantly, falling from 0.869 μm for 120-grit to 0.205 μm for 1000-grit.

Table 3. Effect of different sandpaper grits on chemical polishing quality

Grit size of sandpaper	Before polishing *Ra*, μm	After polishing *Ra*, μm	Rate of decrease in roughness, %
120	0.869	0.720	17.1
320	0.388	0.304	21.6
600	0.257	0.151	41.2
1000	0.205	0.135	34.1

Following chemical polishing, the *Ra* values of all specimens decreased, but the extent of this reduction was closely related to the initial surface condition. When pre-treatment was limited to 120-grit, the *Ra* value remained as high as 0.72 μm after chemical polishing, with a roughness reduction rate of 17.1 %; SEM observation revealed a large number of deep scratches on the surface that had not been completely eliminated (Fig. 7 a). Following 320-grit pre-treatment, the *Ra* value decreased to 0.304 μm; while the depth of the scratches diminished, their number remained considerable (Fig. 7 b). At 600-grit, *Ra* further decreased to 0.151 μm, with a roughness reduction rate of 41.2 %. Surface scratches had almost disappeared (Fig. 7 c);

continuing to 1000-grit resulted in only a slight improvement in the *Ra* value after polishing, with the enhancement effect no longer being significant.

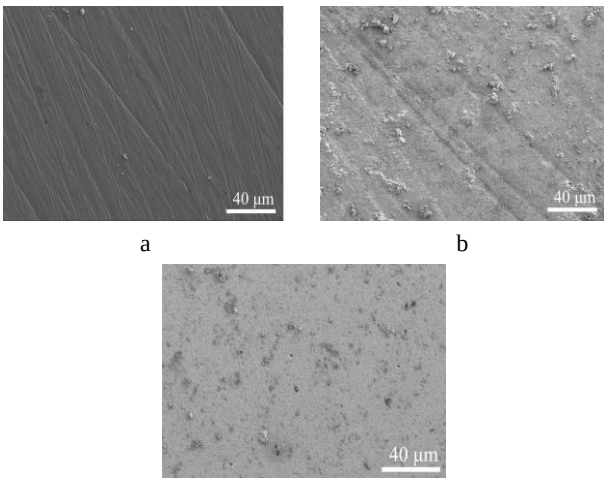

Fig. 7. Effect of pre-grinding grit on polished surface morphology: a – 120 grit; b – 320 grit; c – 600 grit

Taking into account both time efficiency and surface quality, 600-grit sandpaper can be considered a relatively economical and reasonable endpoint for pre-treatment.

3.5. The effect of polishing on the microstructure of P91 steel

The microstructure of P91 steel exhibits significant variations depending on the sample preparation technique. Fig. 8 shows the microstructure under different processes using a fixed polishing solution formulation and an aqueous solution of ferric chloride and hydrochloric acid as the etchant.

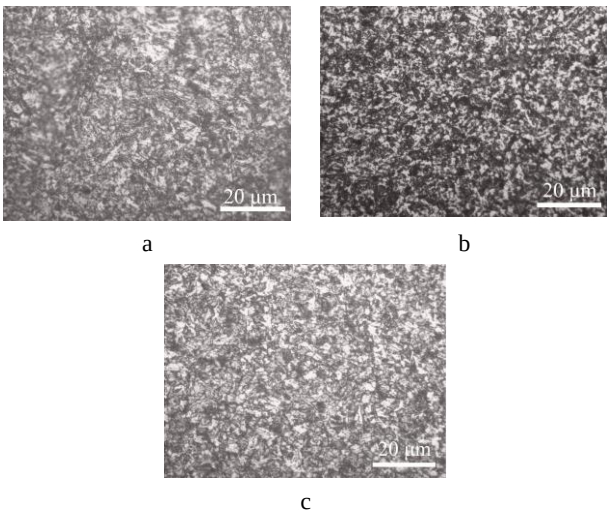

Fig. 8. Metallographic structure under different process conditions: a – insufficient polishing; b – excessive corrosion; c – after optimizations

In Fig. 8 a, insufficient polishing leaves a thick machining deformation layer and deep scratches, obscuring the true martensitic structure. Conversely, prolonged polishing (Fig. 8 b) induces excessive etching and irregular pitting, which disrupts the lamellar structure and causes carbide particle detachment, rendering the specimen unsuitable for quantitative analysis. In contrast, Fig. 8 c demonstrates a standardized metallographic structure. Following optimal polishing and moderate etching, the surface is free of residual deformation layers and excessive etching signs, with distinct tempered martensite lamellae and uniformly dispersed carbides. This high-resolution morphology aligns well with the proposed mechanism of synergistic oxidation, complexation, and dissolution detailed in Section 2.2. The structural integrity indicates that the balance between H_2O_2-driven activation and fluoride/oxalate complexation successfully removes the machining deformation layer without causing selective over-corrosion of the matrix or degrading the secondary phase precipitates. Because the precise, unaltered characterization of these subgrains and dispersed precipitates is critical for evaluating the long-term creep strength of P91 steel [21], preserving these features underscores the reliability of this chemical polishing approach. To contextualize these microstructural findings within the broader landscape of metallographic preparation, it is helpful to compare this optimized chemical approach with other experimental methods. Traditional electrochemical polishing of multiphase alloys frequently suffers from edge rounding and selective phase dissolution due to uneven current density [22], which can distort the true microstructure. Similarly, while recent advancements in laser polishing achieve high surface precision, they often introduce heat-affected zones that alter intrinsic material characteristics [23]. In contrast, the optimized chemical formulation provides an excellent topological finish while effectively preserving the stress-free and thermally unaltered state of the P91 steel matrix and its fine precipitates, offering a practical, high-fidelity alternative for rapid on-site microstructural evaluations.

3.6. Effect of etching solutions on the microstructure of P91 steel

Following normalization and tempering, P91 steel typically exhibits a lamellar tempered martensite microstructure, accompanied by a small amount of δ-ferrite and carbide precipitation. To investigate the compatibility of different etching solutions with this polishing solution system, six experimental protocols were designed (Table 4).

Table 4. Experimental protocol

Project	Experimental protocol
No.1	20 ml H_2O_2+1.75 g NH_4HF_2+2.0 g $H_2C_2O_4$+50 ml HCl+5 g $FeCl_3$+100 ml H_2O
No.2	20 ml H_2O_2+1.75 g NH_4HF_2+2.0 g $H_2C_2O_4$+20 ml HCl+100 ml C_2H_6O
No.3	20 ml H_2O_2+1.75 g NH_4HF_2+2.0 g $H_2C_2O_4$+10 ml HNO_3+100 ml C_2H_6O
No.4	20 ml H_2O_2+1.75 g NH_4HF_2+2.0 g $H_2C_2O_4$+10 ml HNO_3+30 ml HCl
No.5	20 ml H_2O_2+1.75 g NH_4HF_2+2.0 g $H_2C_2O_4$+30 ml HNO_3+10 ml HCl+90 ml C_2H_6O
No.6	20 ml H_2O_2+1.75 g NH_4HF_2+2.0 g $H_2C_2O_4$

No. 6 uses only polishing solution and no longer employs any additional etching agents. The microstructural morphology of the specimens under the different protocols

was subsequently observed using a metallographic microscope; the results are shown in Fig. 9. Comparative analysis reveals that No. 2 (HCl – anhydrous ethanol) yields the optimal microstructural visualization, presenting distinct martensitic lamellae and high grain boundary resolution ideal for metallographic grading. No. 1, 3, and 5 provided moderate visibility but lacked optimal contrast and uniformity. No. 6 (polishing solution only) exhibited faint contours due to mild residual chemical action, whereas No. 4 produced the poorest, heavily blurred results due to aggressive over-etching.

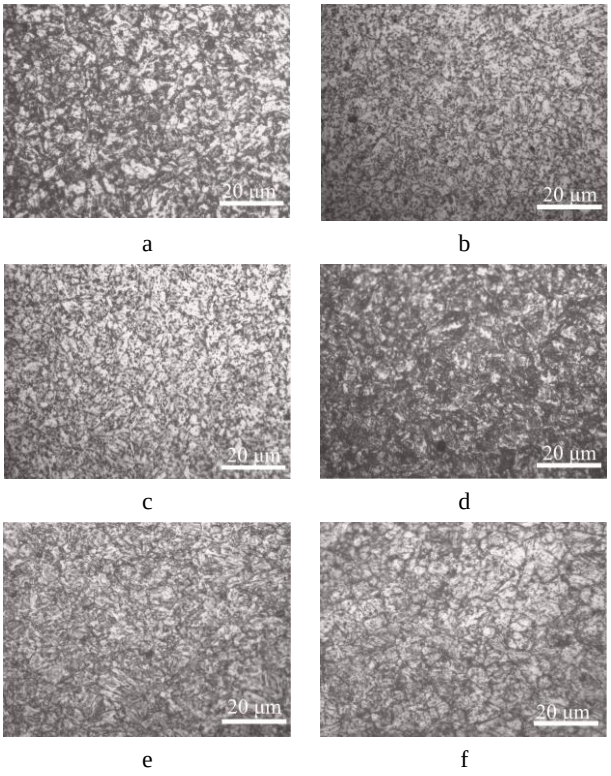

Fig. 9. Metallographic structure under different schemes: a – No. 1; b – No. 2; c – No. 3; d – No. 4; e – No. 5; f – No. 6

A comprehensive comparison reveals that the hydrochloric acid–anhydrous ethanol etching solution is best suited for use with the polishing solution employed in this study. Furthermore, compared to conventional aqueous etchants (which often result in blurred boundaries and aggressive pitting), the clear microstructural revelation achieved by No. 2 highlights the importance of controlling localized corrosion rates in high-alloy steels [24]. By moderating the dissociation rate of acidic ions, the ethanol carrier functions as a buffered system that selectively reveals the martensitic matrix and grain boundaries. This approach prevents severe matrix degradation or dislodgement of fine carbide precipitates typically associated with aggressive aqueous mixtures, providing a more reliable visualization for metallographic grading.

3.7. Micro-compositional validation of the etched surface

The micro-compositional stability of the etched surface is a critical indicator of metallographic preparation quality. To quantitatively investigate the elemental distribution and structural integrity of the P91 steel after optimal etching (Protocol No. 2), high-resolution EDX point analysis was performed. As illustrated in Fig. 10, analytical spots were systematically positioned to capture distinct microstructural features, including the continuous martensitic matrix and the boundary precipitates.

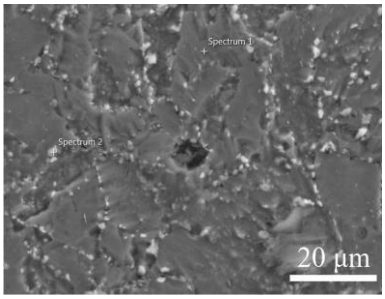

Fig. 10. Targeted analytical spots on the optimally etched P91 steel

The acquired point spectra confirm that the optimized preparation process does not induce preferential elemental dissolution. Analysis of the flat matrix region (Spectrum 1, Fig. 11 a) revealed a stable compositional balance primarily consisting of Fe (89.98 wt.%) and Cr (7.61 wt.%), along with expected trace alloying elements such as Mo (0.25 wt.%) and V (0.15 wt.%).

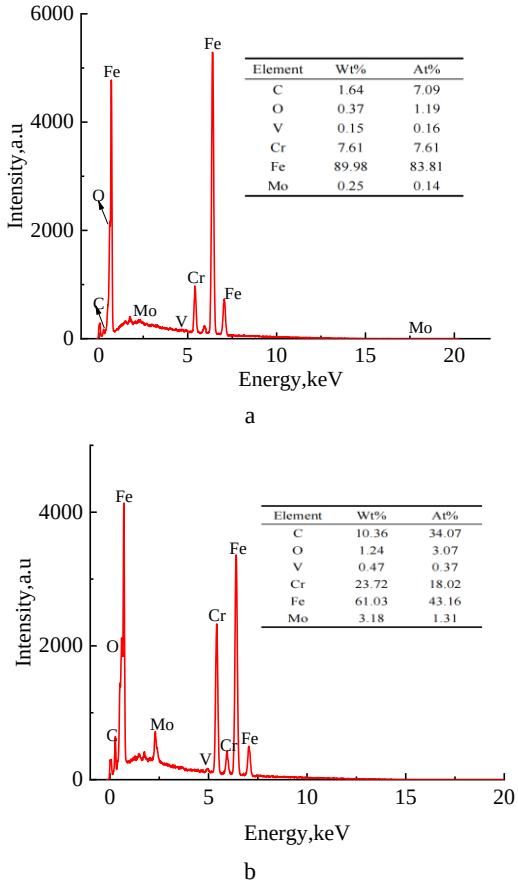

Fig. 11. EDX point analysis spectra of the optimally etched surface: a – intact martensitic matrix (Spectrum 1); b – preserved Cr-rich carbide (Spectrum 2)

This proportional retention of matrix elements confirms that no selective leaching or severe elemental depletion occurred in the bulk material. Furthermore, targeted analysis of the bright secondary-phase particles confirmed their intact preservation. Spectrum 2 (Fig. 11 b), focused directly

on a boundary precipitate, exhibited a significant enrichment in Cr (23.72 wt.%), C (10.36 wt.%), and Mo (3.18 wt.%). This distinct elemental signature indicates that the particle is a Cr-Mo-rich carbide, which is a critical strengthening phase for the high-temperature creep resistance of P91 steel.

While conventional aggressive aqueous etchants frequently cause matrix over-etching and the subsequent dislodgement or compositional degradation of fine precipitates, the EDX results indicate that the optimized ethanol-buffered etchant effectively mitigates these issues. The process selectively reveals the martensitic matrix while largely preserving the micro-alloyed precipitates, providing a high-fidelity, non-destructive surface for accurate microstructural characterization.

4. CONCLUSIONS

This study systematically investigated the optimization of chemical polishing processes and the characterization of microstructures to address the requirements for improving the surface quality of P91 steel tubes and preparing metallographic specimens. The following conclusions were drawn:

1. A full factorial experiment was conducted to determine the optimal formulation for the P91 steel chemical polishing solution: 20 ml hydrogen peroxide, 1.75 g ammonium hydrogen fluoride, 2.0 g oxalic acid, and 25 ml deionized water. Based on range analysis, the order of influence of each factor is: hydrogen peroxide > ammonium hydrogen fluoride > oxalic acid. While ensuring high dissolution efficiency, this formulation achieves a dynamic equilibrium in reaction rate through the chelation of metal ions by oxalic acid and the surface activation by ammonium hydrogen fluoride, thereby preventing over-corrosion.
2. Optimization of process parameters indicates that a polishing temperature of 25 °C and a duration of 120 s are the optimal conditions. Too low a temperature results in a sluggish reaction, while too high a temperature accelerates the decomposition of hydrogen peroxide, causing surface pitting; insufficient time leads to an incomplete reaction and failure to remove scratches, while excessive time causes preferential corrosion of the structure.
3. The grit size of the sandpaper used in the pre-treatment has a decisive influence on the final quality. Experiments indicate that 600-grit sandpaper is the most economical and effective final step in the pre-treatment for chemical polishing. If the grit size is too low, deep scratches are difficult to remove; if it is too high, the improvement in efficiency is limited, increasing time costs.
4. A comparison of six different experimental protocols revealed that No.2 (20 ml hydrochloric acid + 100 ml anhydrous ethanol) is best suited to this polishing solution. This combination clearly and consistently reveals the lamellar tempered martensite structure of P91 steel, facilitating the grading of the microstructure and laying the methodological foundation for establishing a comprehensive metallographic inspection system.
5. Micro-compositional validations using SEM and EDX confirm that the optimal polishing process effectively breaches the temporary chromium-rich passivation layer to maintain a steady-state dissolution. Furthermore, the ethanol-buffered etching solution selectively reveals the martensitic matrix while successfully preserving critical boundary precipitates (such as Cr-rich carbides) without inducing elemental depletion or matrix degradation.

Acknowledgments

The author sincerely appreciates the valuable guidance and careful supervision provided by the supervisor. Gratitude is also extended to the colleagues and classmates in the research group for their valuable suggestions and assistance in the experiment and simulation. Thanks to the relevant institutions and platforms for providing experimental conditions and data support. Meanwhile, the author would like to express heartfelt thanks to the family for their constant support and understanding during the research.

REFERENCES

1. **Sun, X., Che, C., Qian, G., Wang, X.** Microstructure, Hardness and Creep Properties for P91 Steel after Long-Term Service in a Ultra-Supercritical Power Plant *International Journal of Pressure Vessels and Piping* 212 2024: pp. 105330. https://doi.org/10.1016/j.ijpvp.2024.105330
2. **Guguloth, K., Roy, N.** Creep Deformation Behavior of 9Cr1MoVNb (ASME Grade 91) Steel *Materials Science and Engineering: A* 680 2017: pp. 388 – 404. https://doi.org/10.1016/j.msea.2016.10.112
3. **Vaishali, P., Shankar, V., Bhakar, A., Rai, S.** Unravelling the Subgrain Stabilities of Microstructures across P91 Steel Weld Joint under Creep-Fatigue Interaction Loading Waveforms through EBSD and Synchrotron Based XRD Studies *Materials Characterization* 224 2025: pp. 115062. https://doi.org/10.1016/j.matchar.2025.115062
4. **Wang, J., Lu, S., Li, Y., Hu, Q., Rong, L., Li, D.** Cold Cracking Sensitivity of a Newly Developed $9Cr_2WVTa$ Steel *Journal of Materials Engineering and Performance* 26 (1) 2017: pp. 258 – 267. https://doi.org/10.1007/s11665-016-2432-6
5. **Li, Y., Lou, J., Ju, H., Lin, L.** Impact Toughness of Heat-Affected Zones of 11Cr Heat-Resistant Steels *Acta Metallurgica Sinica (English Letters)* 33 (6) 2020: pp. 821 – 827. https://doi.org/10.1007/s40195-020-01014-2
6. **Ashrafi, H., Shamanian, M., Emadi, R., Ghassemali, E.** Void Formation and Plastic Deformation Mechanism of a Cold-Rolled Dual-Phase Steel During Tension *Acta Metallurgica Sinica (English Letters)* 33 (2) 2020: pp. 299 – 306. https://doi.org/10.1007/s40195-019-00967-3
7. **Sun, X., Wang, X.** The Influence of Coupling Effect between Stress and High Temperature on the Degradation of Microstructure and Hardness in P91 Steel *Materials & Design* 244 2024: pp. 113208. https://doi.org/10.1016/j.matdes.2024.113208
8. **Karzina, J.S., Shvetsov, O.V.** Analysis of Causes of Corrosion Damage to Internal Surface of Stainless Steel Heat Exchanger Tubes *Key Engineering Materials* 943

2023: pp. 71 – 77.
https://doi.org/10.4028/p-oor37i

9. **Singh Shergill, R., Perez, F., Abdalla, A., Anil Patel, B.** Comparing Electrochemical Pre-Treated 3D Printed Native and Mechanically Polished Electrode Surfaces for Analytical Sensing *Journal of Electroanalytical Chemistry* 905 2022: pp. 115994.
https://doi.org/10.1016/j.jelechem.2021.115994
10. **Arthanari, S., Park, J.E., Heo, J.S., Cho, D.H., Yang, M., Hwang, J.S., Lee, H.** Laser Surface Polishing of 3D Printed Polylactic Acid (PLA) with Different Levels of Absorption *Journal of Manufacturing Processes* 98 2023: pp. 265 – 276.
https://doi.org/10.1016/j.jmapro.2023.05.034
11. **Chmielewska, A., Jahadakbar, A., Wysocki, B., Elahinia, M., Święszkowski, W., Dean, D.** Chemical Polishing of Additively Manufactured, Porous, Nickel–Titanium Skeletal Fixation Plates *3D Printing and Additive Manufacturing* 9 (4) 2022: pp. 269 – 277.
https://doi.org/10.1089/3dp.2020.0209
12. **Wang, S.F., Wang, Y., Wen, J.C., Suo, H.L., Liu, Z.Z., Suo, W.H., Zhao, C.C.** Study on Electrochemical Polishing of TC4 Alloy *Materials Research Express* 8 (10) 2021: pp. 106520.
https://doi.org/10.1088/2053-1591/ac1f4c
13. **Peng, W., Cheng, C., Hu, J., Liu, Y., Li, M., Song, C., Shi, W.** Evaluation of Treatment Effect and Mechanism Analysis of Ti6AL4V Porous Scaffolds Prepared by Selective Laser Melting with Different Chemical Polishing Processes *3D Printing and Additive Manufacturing* 11 (5) 2024: pp. 1746 – 1757.
https://doi.org/10.1089/3dp.2023.0103
14. **Li, F., Li, S., Tong, H., Xu, H., Wang, Y.** The Application of Chemical Polishing in TEM Sample Preparation of Zirconium Alloys *Materials* 13 (5) 2020: pp. 1036.
https://doi.org/10.3390/ma13051036
15. **Tyagi, P., Goulet, T., Riso, C., Garcia-Moreno, F.** Reducing Surface Roughness by Chemical Polishing of Additively Manufactured 3D Printed 316 Stainless Steel Components *The International Journal of Advanced Manufacturing Technology* 100 (9) 2019: pp. 2895 – 2900.
https://doi.org/10.1007/s00170-018-2890-0
16. **Weng, J., Lin, R., Rong, X.** Study on Polishing Slurry of Hydrogen Peroxide-Oxalic Acid in CMP 304 Stainless Steel *In MATEC Web of Conferences* 327 2020: pp. 02002.
https://doi.org/10.1051/matecconf/202032702002
17. **Xia, J., Zhu, S., He, X., Shen, J., Li, X., Kong, Y., Yao, C.** Effect of Thermal Activation Temperature on Chemical-Mechanical Polishing of Titanium Alloy *Industrial Lubrication and Tribology* 77 (9) 2025: pp. 1528 – 1538.
https://doi.org/10.1108/ILT-05-2024-0167
18. **He, M.F., Wang, H., Jiang, H., Zhao, S., Pan, D.** Effect of Hydrogen Peroxide Concentration on Surface Properties of Ni–Cr Alloys *Transactions of Nonferrous Metals Society of China* 26 (5) 2016: pp. 1353 – 1358.
https://doi.org/10.1016/S1003-6326(16)64238-3
19. **Olsson, C.O.A., Landolt, D.** Passive Films on Stainless Steels – Chemistry, Structure and Growth *Electrochimica Acta* 48 (9) 2003: pp. 1093 – 1104.
https://doi.org/10.1016/S0013-4686(02)00841-1
20. **Frankel, G.S.** Pitting Corrosion of Metals: A Review of the Critical Factors *Journal of The Electrochemical Society* 145 (6) 1998: pp. 2186.
https://doi.org/10.1149/1.1838615
21. **Hald J.** Microstructure and Long-Term Creep Properties of 9–12% Cr Steels *International Journal of Pressure Vessels and Piping* 85 (1) 2008: pp. 30 – 37.
https://doi.org/10.1016/j.ijpvp.2007.06.010
22. **Han, W., Fang, F.** Fundamental Aspects and Recent Developments in Electropolishing *International Journal of Machine Tools and Manufacture* 139 2019: pp. 1 – 23.
https://doi.org/10.1016/j.ijmachtools.2019.01.001
23. **Krishnan, A., Fang, F.** Review on Mechanism and Process of Surface Polishing Using Lasers *Frontiers of Mechanical Engineering* 14 (3) 2019: pp. 299 – 319.
https://doi.org/10.1007/s11465-019-0535-0
24. **Forcellese, P., Mancia, T., Simoncini, M., Bellezze, T.** Characterization of Microstructure and Localized Corrosion Resistance of Heat-Treated 17-4 PH Stainless Steel Fabricated by Material Extrusion *Metals* 15 (2) 2025: pp. 137.
https://doi.org/10.3390/met15020137